# Integrating green-shoulder indices from hyperspectral drone imagery and sap flow monitoring to assess water dynamics in healthy and bark beetle-infested trees

Luiz Henrique Elias Cosimo[1], Jose Gutierrez Lopez[2], Eva Lindberg[1], Zuosinan Chen[3], Langning Huo[1]

[1] Department of Forest Resource Management, Swedish University of Agricultural Sciences, S-901 83 Umeå, Sweden – {luiz.cosimo, eva.lindberg, langning.huo}@slu.se
[2] Department of Forest Ecology and Management, Swedish University of Agricultural Sciences, S-901 83 Umeå, Sweden – jose.lopez@slu.se
[3] Department of Water, Energy and Environmental Engineering, University of Oulu, FI-90014 Oulu, Finland – zuosinan.chen@oulu.fi

**Keywords:** hyperspectral imagery, sap flow, green-shoulder indices, bark beetle infestation, forest health

**Abstract**

Accurate detection of tree physiological stress is essential for understanding health decline and improving disturbance monitoring. Tree stress if often linked to hydraulic dysfunction, yet detecting the onset of this process at canopy scale remains challenging. In this study, we investigated whether spectral indices derived from the green-shoulder region can capture changes in tree hydraulic functioning. We combined hyperspectral drone imagery with continuous sap flow monitoring in a Norway spruce (*Picea abies*) forest in southern Sweden undergoing bark beetle infestation. Sap flux density (Js) was measured at three depths (1, 2, and 3 cm into the sapwood) to characterize hydraulic responses during infestation progression between weeks 16 and 32 of 2023. During the same period, seven airborne hyperspectral acquisitions were conducted using a VNIR sensor. We calculated indices from the Photochemical Reflectance Index (PRI) and Green Shoulder Curvature Ratio (GSCR) families and examined their relationships with weekly sap flow dynamics. We observed Js declines in one of more sensor depths in infested trees, occasionally leading to complete conductivity collapse and, consequently, tree mortality. Green-shoulder indices strongly responded to Js decline from week 26, especially in the outer sensor depth, indicating that spectral signals tracked changes in tree water transport. Our findings demonstrate that green-shoulder indices can reflect underlying hydraulic processes and provide a fast, scalable approach for monitoring hydraulic stress to support forest health monitoring.

## 1. Introduction

European forests have suffered extensive losses from biotic and abiotic disturbances in recent decades, leading to increased tree mortality, large reductions in standing biomass and timber resources, and significant declines in forest carbon storage and sequestration capacity (Patacca et al., 2023; Romeiro et al., 2022; Seidl et al., 2014). Furthermore, these events are highly likely to increase in the coming decades considering current climate change scenarios (Grünig et al., 2026). In this context, effective and efficient tools to assess forest health and identify stressed trees and stands are becoming increasingly important to mitigate negative impacts and support sustainable forest management.

Ecophysiological measurements such as sap flow can provide detailed insights into tree hydraulic functioning and enable real-time identification of stress onset and progression (Mantova et al., 2022; Tams et al., 2024). As such, these measurements provide valuable ground information in plant stress studies. However, this approach requires costly instrumentation, which is typically limited to a small number of sampled trees.

Remote sensing technologies, by contrast, offer the possibility to scale tree health monitoring across larger spatial extents. Realizing this potential, however, depends on robust spectral indicators that reliably reflect hydraulic functioning. Among the many candidates in the literature, previous research suggests that spectral indicators derived from the green-shoulder region (the slope between the blue absorption feature and the green reflectance peak, ~490-560 nm) may be suitable for this purpose.

The Photochemical Reflectance Indices (PRIs) were the first spectral indicators developed from the this region, designed to capture changes in photosynthetic light-use efficiency associated with photoprotective pigment dynamics in healthy and stressed plants (Gamon et al., 1992). These indices exploit reflectance changes at 531 nm, associated with pigment conversions in the xanthophyll cycle activated for photoprotection, using 550 or 570 nm as reference wavelengths for normalization (Gamon et al., 1992; Peñuelas et al., 1994, 1995).

More recently, additional indicators from this spectral region have been proposed for detecting Norway spruce (*Picea abies* [L.] Karst) infested with bark beetles (*Ips typographus* L.). Using spectral derivative curves, Huo et al. (2024) showed that subtle tree vitality decline resulted in shifts in inflection (~520 and ~545 nm) and curvature (~530 nm) points. Building on these observations, the authors developed the Green Shoulder Curvature Ratio (GSCR) indices. They subsequently proposed simplified versions using a limited number of spectral bands and algebraic operations that approximate the relationships observed in the derivative curves, allowing these indices to be implemented with multispectral sensors. These GSCR indices have shown strong performance in detecting bark beetle-infested trees, as demonstrated by Huo et al. (2024) and a subsequent study conducted in Sweden (Cosimo et al., 2025).

In this study, we use sap flow monitoring to demonstrate that tree mortality in infested trees results from hydraulic dysfunction following beetle colonization. Based on this finding and considering the potential of green-shoulder indices (GSI) to detect infestations, we hypothesize that GSI are closely linked to tree hydraulic functioning and respond to temporal changes in water transport. To test this hypothesis, we combine hyperspectral drone imagery with continuous sap flow monitoring to:

1. assess whether GSI correlate with sap flow measurements and capture weekly variations in tree water transport.
2. examine how GSI respond to sap flow changes following bark beetle infestation.
3. evaluate whether sensor depth influences these relationships and whether GSI are more strongly associated with specific sensor depths.

## 2. Material and methods

The study was conducted in Remningstorp, southern Sweden (58°27’18’’, 13°39’8’’E), within a controlled field experiment established to investigate bark beetle dynamics and tree physiological responses. The experimental site consisted of 24 circular field plots with a radius of 15 m, distributed across four forest stands. The stands were even-aged, mature forests dominated by Norway spruce, representative of managed spruce forests common in southern Sweden. The position of all trees within each plot was mapped in the field using a high-accuracy GNSS system, enabling precise spatial alignment between field measurements and remotely sensed data.

During the growing season of 2023, field surveys were conducted weekly to record signs of bark beetle infestation. These surveys included visual assessments of typical infestation indicators such as entrance holes, boring dust, and crown discoloration, allowing the timing and progression of infestations to be monitored throughout the season.

To investigate tree hydraulic responses, sap flow monitoring stations were installed in two field plots located in different stands (Figure 1), namely Plot 1 and Plot 2. Each monitoring station measured sap flow in eight trees, providing a total of 16 monitored individuals. Sensors were installed at breast height (1.3 m) on the south-facing side of each stem. For clarity, trees are hereafter referred to as tree1–tree8 within each plot. Sap flow was monitored at the depths of 1, 2, and 3 cm, which we denoted as the outer, middle, and inner sensor depths, respectively. Data were recorded continuously at 15-minute intervals, allowing high temporal resolution observations of tree water transport dynamics over the growing season.

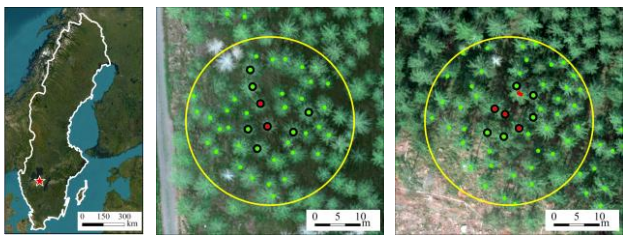

(a) (b) (c)

Figure 1. Study area location and layout of the field plots used for sap flow monitoring. (a) Location of the experimental site in Remningstorp, southern Sweden (red star). (b–c) Spatial distribution of trees in the two monitored plots (Plot 1 and Plot 2, respectively). Green dots indicate healthy trees, red dots indicate infested trees, and black circles mark trees equipped with sap flow sensors.

Sap flux density (Js) was estimated using the maximum heat ratio method (Lopez et al., 2021) and used to assess hydraulic responses to bark beetle infestation. Among the monitored spruce trees, five were successfully colonized by bark beetles (Table 1), of which four died in the same year and one in the following year. Sensors producing malfunctioning or noisy measurements were excluded from the analysis. In Plot 1, the outer sensor depth of tree5 was excluded, data from tree6 prior to week 21 were discarded, and measurements after week 31 were excluded for all trees. In Plot 2, all measurements from tree4 were discarded, as well as the depth outer sensor data from tree3.

| | Status | n | DBH (mean ± sd, in cm) |
|---|---|---|---|
| Plot 1 | Healthy | 6 | 27.6 ± 3.53 |
| | Infested | 2 | 21.1 ± 3.68 |
| Plot 2 | Healthy | 5 | 23.9 ± 2.2 |
| | Infested | 3 | 27.4 ± 6.27 |

Table 1. Plots with sap flow monitoring. n = number of trees; DBH = diameter at breast height; sd = standard deviation.

While reductions in daily Js may indicate hydraulic stress, interpreting absolute declines in infested trees alone can be misleading. Js can naturally fluctuate in both healthy and infested trees in response to daily and even hourly environmental variability (e.g., dynamic atmospheric demand and soil moisture vary with different weather conditions). Therefore, identifying infestation-induced hydraulic stress needs to exclude the environmentally driven hydraulic fluctuation.

To do so, we tested the consistency of Js patterns in each field plot at a weekly scale. We assumed that without infestation, all trees in the same plot should present similar behaviours in Js since they were exposed to the same environmental conditions that strongly and sensitively regulate Js patterns. Meanwhile, trees with hydraulic dysfunction would show deviating patterns. Each tree (both healthy and infested) was paired with all healthy trees within the same field plot and the Pearson correlation coefficient (r) was calculated for each pair on a weekly basis and for each sensor depth. Subsequently, for each tree and sensor depth, we computed a mean weekly r value by averaging the correlation coefficients obtained from all pairwise comparisons with healthy trees. For each week where all Js records were available, there were 672 observations for each pair (96 logged values per day). We considered that an infested tree started to present signs of hydraulic stress when r (from *infested vs healthy* pairs) dropped from one week and another, while r for healthy trees (from *healthy vs healthy* pairs) remained stably high.

Hyperspectral data were acquired using a SPECIM AFX10-VNIR camera mounted on an Alta X multirotor drone. The sensor recorded 224 spectral bands across 400–1,000 nm. Flights were conducted at 100 m altitude and resulted in a ground sampling distance (GSD) of approximately 7 cm. A total of seven flights were carried out during the 2023 growing season (Figure 2). Radiometric calibration and geo-rectification were performed in CaliGeoPRO software. Reflectance was estimated using ground targets with near-Lambertian properties placed in the scene for every flight.

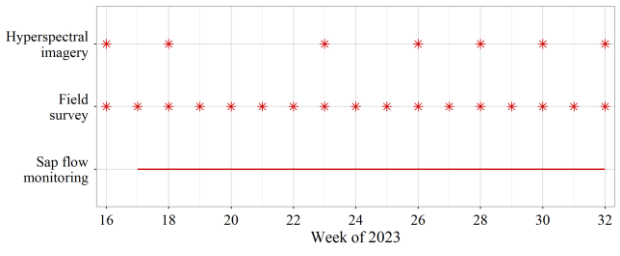


Figure 2. Timeframe of data collection for the different datasets.

| Index | Notation | Definition | Reference |
|---|---|---|---|
| Photochemical Reflectance Index 550/531 | $PRI_{550/531}$ | $\frac{R_{550}-R_{531}}{R_{550}+R_{531}}$ | Gamon et al. (1992) |
| Photochemical Reflectance Index 531/570 | $PRI_{531/570}$ | $\frac{R_{531}-R_{570}}{R_{531}+R_{570}}$ | Peñuelas et al. (1995) |
| Green Shoulder Curvature Ratio 1 MS | $GSCR1_{MS}$ | $\frac{R_{550}-R_{530}}{R_{530}-\left(\frac{R_{550}+R_{490}}{2}\right)}$ | Huo et al. (2024) |
| Green Shoulder Curvature Ratio 2 MS | $GSCR2_{MS}$ | $\frac{R_{550}-R_{530}}{(R_{530}-R_{490})*\left(R_{530}-\frac{R_{550}+R_{490}}{2}\right)}$ | Huo et al. (2024) |
| Green Shoulder Curvature Ratio 1 2026 | $GSCR1_{2026}$ | $\ln\left(\left\lvert\frac{R_{550}-R_{530}+\alpha}{R_{530}-\left(\frac{R_{550}+R_{490}}{2}\right)+\alpha}\right\rvert\right)$ | Adapted from Huo et al. (2024) |
| Green Shoulder Curvature Ratio 2 2026 | $GSCR2_{2026}$ | $\ln\left(\left\lvert\frac{(R_{550}-R_{530}+\alpha)^2}{(R_{530}-R_{490})*\left(R_{530}-\frac{R_{550}+R_{490}}{2}+\alpha\right)}\right\rvert\right)$ | Adapted from Huo et al. (2024) |

Table 2. List of green-shoulder indices calculated, including their notations, definitions, and references. R indicates reflectance at a given wavelength. Mean reflectance values using 20 nm spectral bins centred on each target wavelength were used for calculations.

A local maxima detection algorithm was applied to the green band (~550 nm) to identify treetops, which were then used as markers in a marker-controlled watershed segmentation algorithm to delineate individual tree crowns. The resulting treetop positions were spatially matched with the field-mapped locations of trees equipped with sap flow sensors. To minimize the influence of background elements such as shadows or understory vegetation, a threshold applied to the green band was used to mask non-canopy pixels. The mean reflectance at each band was then calculated from the 25% brightest pixels within a 1 m buffer around each treetop, constrained by the segment boundaries (Huo et al., 2025).

We calculated six spectral indices from the PRI and GSCR families: $GSCR1_{MS}$, $GSCR2_{MS}$, $GSCR1_{2026}$, $GSCR2_{2026}$, $PRI_{550/531}$, and $PRI_{531/570}$ (Table 2). $GSCR1_{2026}$ and $GSCR2_{2026}$ are adaptations from the simplified indices proposed by Huo et al. (2024) designed to avoid extreme values that occur when terms in the equations approach zero. To address this, a constant term ($\alpha$ = 0.15) was added, and the natural logarithm of the absolute value was applied.

To examine the relationship between spectral signals and tree hydraulic activity, we fitted simple linear regression models with index values as the explanatory variables and the weekly cumulative Js as the response variable. The weekly cumulative Js was used to account for the temporal mismatch between the continuous sap flow measurements and the discrete drone acquisitions.

The regressions were performed separately for each sensor depth (outer, middle, inner) as well as for all depths combined (i.e., cumulative Js across all depths), and independently for each flight week. To evaluate whether these relationships were consistent across the season, we additionally pooled observations from all weeks and refitted the regressions without separating by week.

To account for potential delayed spectral responses to hydraulic changes, we also tested regression models using lagged values, specifically the weekly cumulative Js from the two weeks preceding each drone flight. The coefficient of determination ($R^2$) was used as the primary metric to compare the strength of the relationships between spectral indices and sap flow measurements across weeks and sensor depths.

## 3. Results and discussion

In infested trees, Js initially exhibited fluctuations comparable to those observed in healthy trees, reflecting shared responses to environmental conditions prior to bark beetle colonization. However, a few weeks after colonization, a pronounced decline in Js occurred that was not followed by recovery (Figure 3), indicating the onset of sustained hydraulic dysfunction.

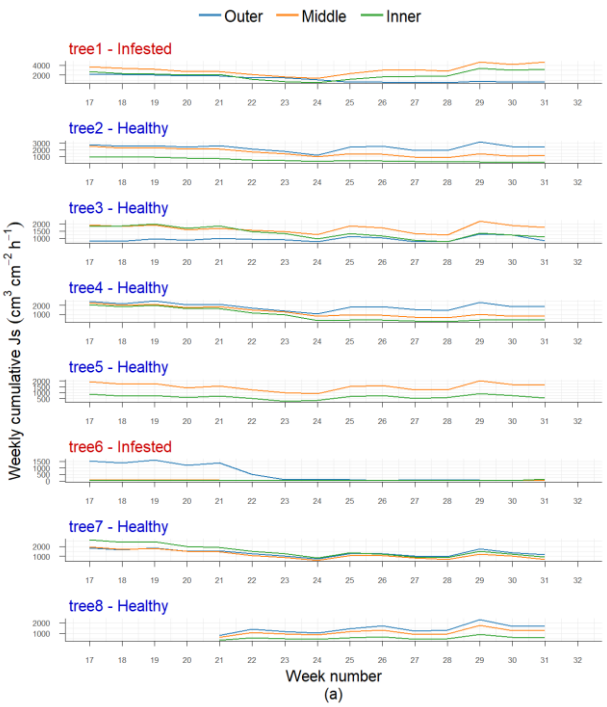

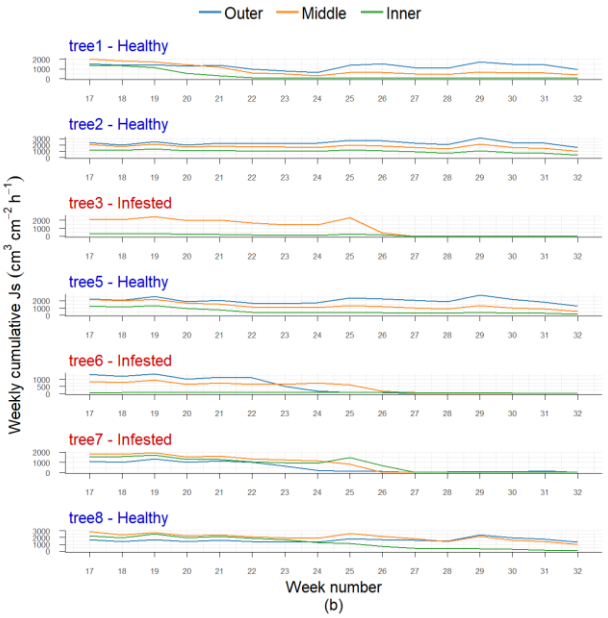


Figure 3. Weekly sum of sap flux density (Js) in different sensor depths (outer, middle, inner) for all instrumented trees in Plot 1 (a) and Plot 2 (b).

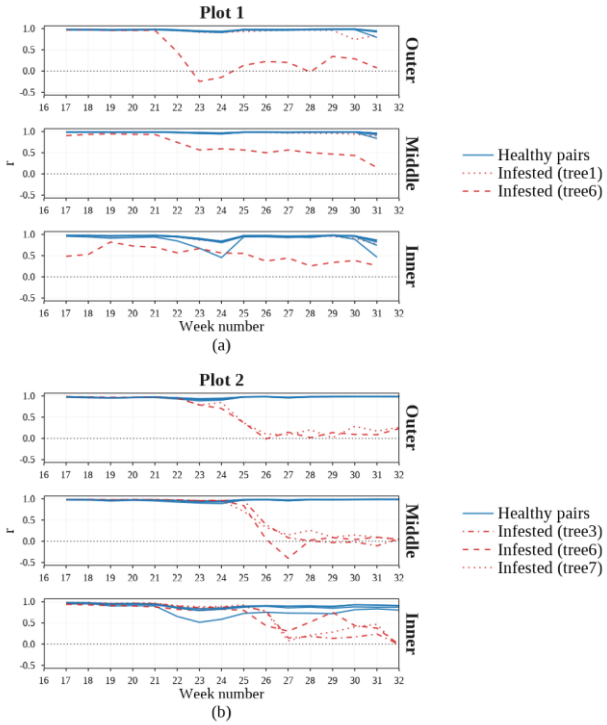


Figure 4. Mean weekly Pearson correlation coefficient (r) between each tree and all healthy trees in the same plot for different sensor depths (outer, middle, inner), for Plot 1 (a) and Plot 2 (b). All *healthy vs healthy* pairs have been merged into a single category to facilitate legend interpretation.

Correlations between infested and healthy trees followed different temporal patterns (Figure 4). During the initial weeks, r values were similarly high, suggesting comparable hydraulic patterns. However, for most infested trees, there was a notable decline in r (e.g., from ~1 to ~0 in 2-4 weeks), especially in the outer sensor depth, indicating hydraulic behaviour deviated from healthy references after bark beetle attacks.

In Plot 1 (Figure 4a), tree6 began to exhibit deviating r values in the outer sensor depth from week 22. In contrast, tree1 maintained high r values throughout the monitoring period, indicating daily patterns consistent with those of healthy trees. Nevertheless, this tree showed a change in Js from week 25 onward (Figure 4a), with outer-depth Js decreasing and remaining relatively stable thereafter, while healthy trees in the same plot exhibited Js increase followed by weekly fluctuations.

In Plot 2 (Figure 4b), tree6 and tree7 began to show subtle declines in r values in the outer sensor depth starting in week 23, followed by a sharp decrease from week 25 onward. Finally, tree3, for which outer-depth data were not available, exhibited declining r values in the middle sensor depth beginning in week 26. Given that the response in the middle depth was similar to that observed in tree6 and tree7, it is likely that tree3 would also have exhibited a decline in the outer depth at an earlier stage, had those measurements been available.

| Plot | Tree | Hole week | Many holes week | Hydraulic stress week | Hydraulic failure week |
|---|---|---|---|---|---|
| 1 | 1 | 23 | 24 | 25 | - |
| 1 | 6 | 19 | 19 | 22 | - |
| 2 | 3 | 23 | 23 | 26 | 27 |
| 2 | 6 | 19 | 21 | 23 | 26 |
| 2 | 7 | 21 | 21 | 23 | 27 |

Table 3. Summary of field symptoms. Hole week = week when bark beetle holes were first recorded. Many holes week = week when >30 holes were recorded. Hydraulic stress = week when the mean correlation with healthy trees started to decline. Hydraulic failure = week when collapse in all sensor depths occurred.

GSI closely tracked infestation progression. At the beginning of the growing season, healthy and infested trees exhibited overlapping GSI values, indicating similar canopy signals. However, in the weeks following bark beetle colonization, GSI values of infested trees progressively diverged from those of healthy individuals (Figure 5), reflecting the development of physiological stress associated with infestation.

$GSCR1_{MS}$ and $GSCR2_{MS}$ maintained substantial overlap between healthy and infested tree values prior to week 23, with a gradual and progressive divergence emerging mainly from week 28. This pattern suggests a temporally coherent separation aligned with infestation progression. In contrast, PRI indices exhibited multiple instances of early separation between healthy and infested trees even before bark beetle colonization (especially in Plot 1), resulting in a higher occurrence of false-positive detections. The degree of deviation between healthy and infested trees in the late weeks was lower for $GSCR1_{2026}$ compared to $GSCR1_{MS}$, indicating reduced extremes and smoother transitions. In contrast, $GSCR2_{2026}$ showed little to no differentiation between healthy and infested trees.

When evaluating the relationship between GSI indices and weekly cumulative Js, weak associations were observed during the initial weeks, when trees were hydraulically stable and Js fluctuations largely reflected environmental variability (Figure 6, Figure 7a). Therefore, GSI were highly insensitive to natural Js variation between trees and weeks.

Nevertheless, as hydraulic dysfunction developed – particularly in the outer sensor depth – strong linear relationships emerged (Figure 6). These relationships became significant from week 26, when $R^2$ values ranged between 0.22 and 0.53 across spectral indices. Based on Table 3, the emergence of these relationships occurred, on average, three weeks after hydraulic stress was first detected in infested trees. These relationships strengthened further as the infestation progressed. For instance, $R^2$ exceeded 0.70 for the relationships between $PRI_{550/531}$, $PRI_{531/570}$, $GSCR2_{MS}$, and $GSCR1_{2026}$ and weekly cumulative Js in the outer sensor depth in weeks 30 and 32 (Figure 6a). The results from regression models fitted for $PRI_{550/531}$ can be visualized in Figure 6a, which was the index with highest $R^2$ in most weeks. Furthermore, these relationships were observed from the combined analysis of data from both field plots, indicating robustness to inter-site differences (e.g., soil moisture, slope, and tree variability).

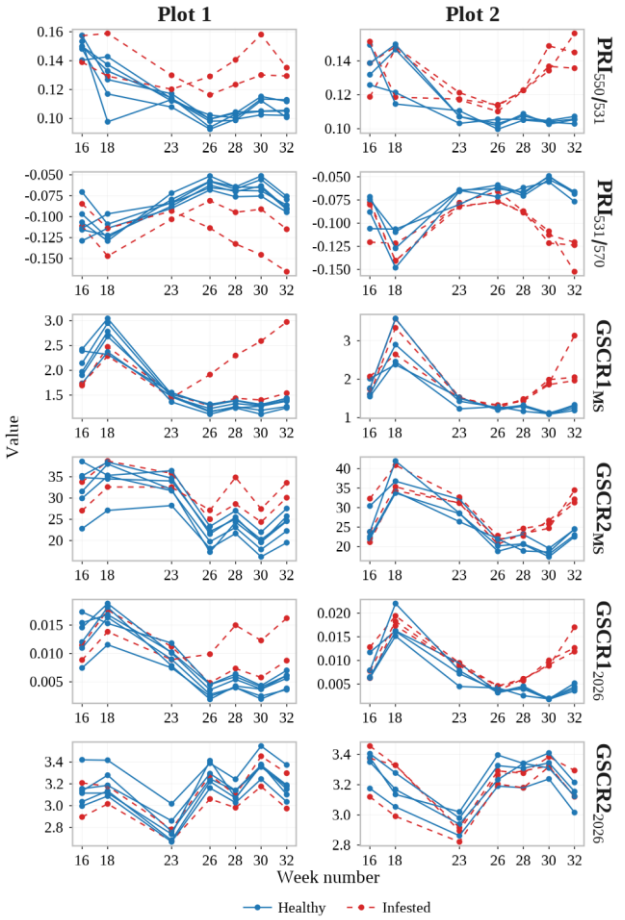


Figure 5. Time series of selected green-shoulder indices, for trees equipped with sap flow sensors in each plot.

Importantly, introducing a 2-week lag in cumulative Js did not substantially improve model performance (Figure 6b). Although lagged relationships remained significant in several cases, their explanatory power was generally comparable to that obtained using same-period Js, particularly during weeks 28–32 when hydraulic decline intensified. This suggests that GSIs can respond well to ongoing hydraulic impairment.

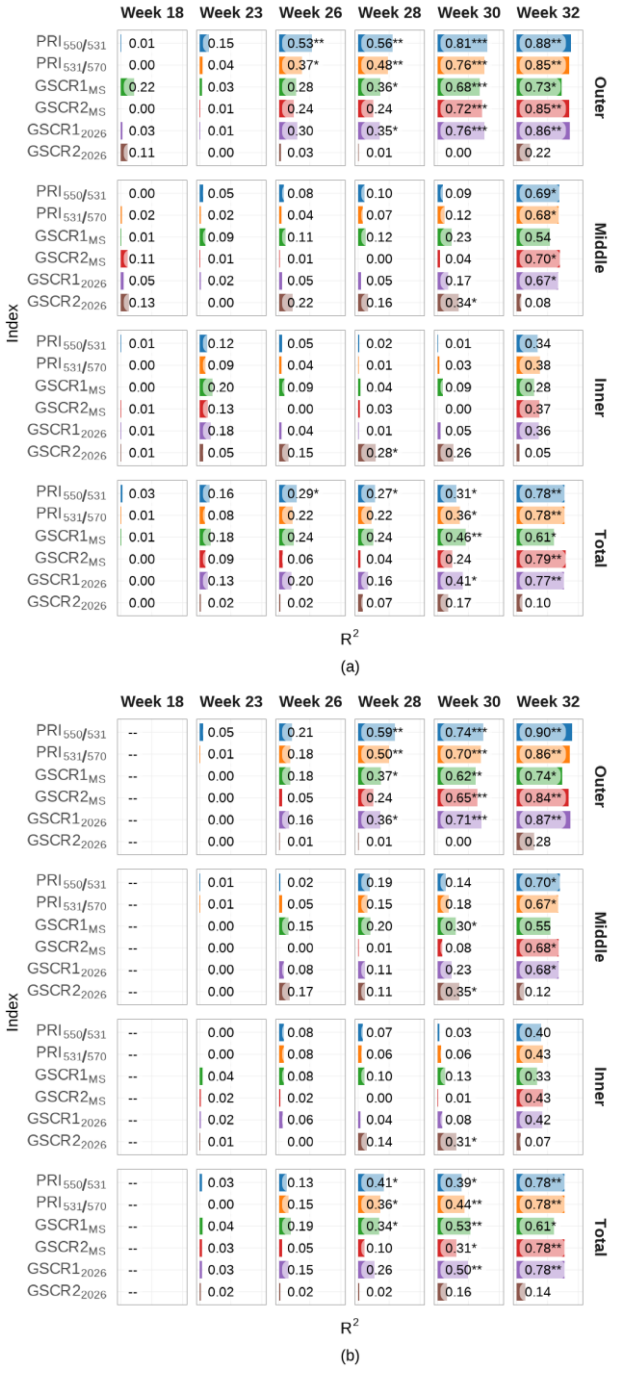


Figure 6. Coefficients of determination ($R^2$) from simple linear regression models relating green-shoulder indices to weekly cumulative sap flux density (Js) measured at different sensor depths. Models were fitted using Js from the same week as hyperspectral image acquisition (a) and from a 2-week lag (b). Analyses were conducted separately for each week and sensor depth (Outer, Middle, Inner), as well as for all depths combined (Total). Asterisks indicate statistically significant relationships (* $p < 0.05$, ** $p < 0.01$, *** $p < 0.001$). In panel (b), sap flux data for the 2-week lag were not available for week 18.

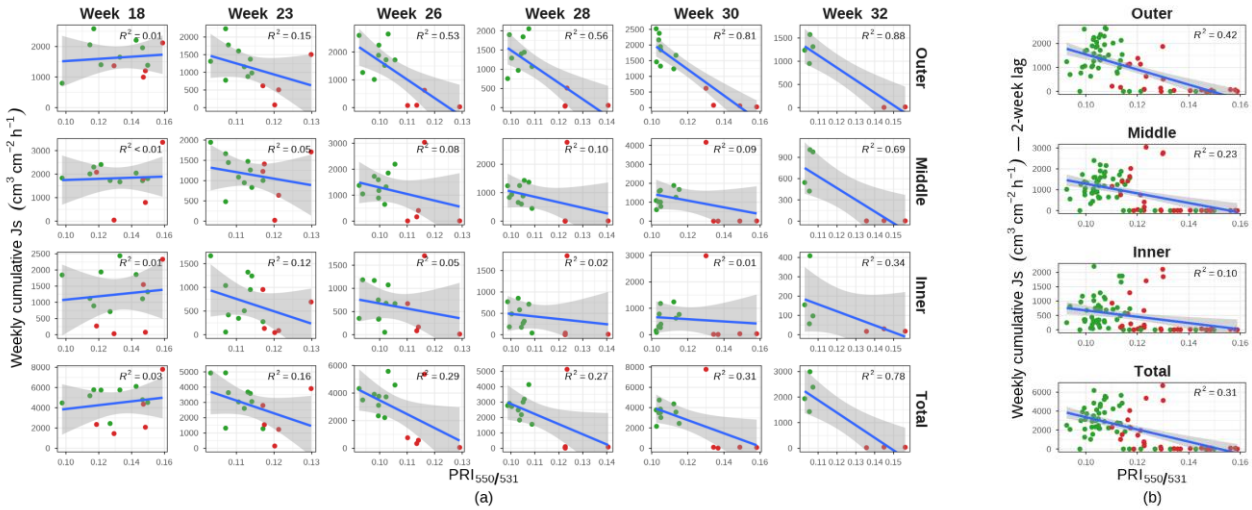


Figure 7. Relationships between $PRI_{550/531}$ and the weekly cumulative sap flux density (Js) across sensor depths. (a) Simple linear regressions between $PRI_{550/531}$ and the weekly cumulative Js, shown by week of hyperspectral image acquisition and sensor depths: Outer, Middle, Inner, and Total (i.e., all depths combined). (b) Simple linear regressions between $PRI_{550/531}$ and the weekly cumulative Js with a 2-week lag pooled across weeks for each sensor depth.

Mechanistically, this behaviour is consistent with the activation of the xanthophyll cycle under hydraulic stress. Reductions in water transport constrain stomatal conductance and carbon assimilation, increasing excess excitation energy in the photosynthetic apparatus (Chaves et al., 2009; Ruban, 2016). To mitigate damage, trees enhance non-photochemical quenching through xanthophyll cycle activity, which alters reflectance in the green-shoulder region (D’Odorico et al., 2025). The strong associations observed between GSIs and Js during periods of hydraulic decline therefore likely reflect this rapid photoprotective adjustment, linking canopy-level spectral properties directly to needle-level responses to hydraulic functioning.

The strongest relationships were consistently observed in the outer sensor depth, which is generally associated with the most hydraulically active sapwood layer and typically the first to experience conductivity loss during stress. Middle and inner depths showed weaker or delayed associations, consistent with sapwood layers with reduced contribution to transpiration and slower hydraulic deterioration.

Collectively, these results demonstrate that GSIs effectively capture the onset of hydraulic stress in near real time, through their sensitivity to photoprotective responses, reinforcing their potential utility for the detection of bark beetle-induced hydraulic dysfunction.

When the temporal structure was removed from the analysis and data were pooled across weeks, the performance of all GSI indices decreased substantially (Table 4, Figure 7b). This reduction in explanatory power is primarily attributable to the weak associations observed during the initial weeks, when trees were hydraulically stable and spectral responses had not yet diverged.

Under these temporally aggregated conditions, weekly cumulative Js was only slightly explained by GSI, particularly for the middle and inner sensor depths. In contrast, when weekly cumulative Js over the preceding two weeks was considered, model performance improved consistently across indices. The strongest relationships were observed in the outer sensor depth, where $PRI_{531/570}$ reached an $R^2$ of 0.46 (Table 4). Similar relationships were also observed for $GSCR1_{MS}$ and $PRI_{550/531}$ (Table 4, Figure 7b).

| Js | Depth | $GSCR1_{Ms}$ | $GSCR2_{Ms}$ | $PRI_{550/531}$ | $PRI_{531/570}$ |
|---|---|---|---|---|---|
| Weekly cumul. Js | out | 0.02 | 0.03 | 0.15*** | 0.11** |
| | mid | 0.01 | 0.04 | 0.00 | 0.00 |
| | inn | 0.05* | 0.05* | 0.01 | 0.02 |
| | tot | 0.01 | 0.01 | 0.02 | 0.01 |
| Weekly cumul. Js (2-week lag) | out | 0.45*** | 0.16*** | 0.42*** | 0.46*** |
| | mid | 0.36*** | 0.07* | 0.23*** | 0.29*** |
| | inn | 0.19*** | 0.02 | 0.10** | 0.14*** |
| | tot | 0.42*** | 0.11** | 0.31*** | 0.39*** |

Table 4. Coefficients of determination ($R^2$) from simple linear regression models relating green-shoulder indices to weekly cumulative sap flux density (Js) measured at different sensor depths. Models were fitted using Js from the same week as hyperspectral image acquisition and from a 2-week lag. Data from all weeks were pooled together, and analyses were conducted separately for each sensor depth (out = Outer, mid= Middle, inn= Inner), as well as for all depths combined (tot = Total). Asterisks indicate statistically significant relationships (* $p < 0.05$, ** $p < 0.01$, *** $p < 0.001$).

These results indicate that, when temporal progression is not explicitly considered, GSIs are more strongly associated with accumulated hydraulic stress than with instantaneous weekly sap flux. The improvement observed with lagged Js suggests that canopy spectral responses integrate hydraulic constraints over short time windows, particularly in the hydraulically active outer sensor depth. However, the moderate $R^2$ values also highlight that temporal dynamics play a critical role in strengthening the linkage between hydraulic dysfunction and spectral response.

Overall, our results indicate that GSIs show strong potential for detecting hydraulic stress, as their temporal dynamics closely track changes in sap flow in infested trees. While the hyperspectral system used in this study is not readily suitable for operational applications due to its high payload, limited flight

time, and complex data processing, PRI and simplified GSCR formulations rely on few spectral bands and therefore offer clear opportunities for operational monitoring using multispectral drone systems. Such approaches could enable the upscaling of tree health assessments across larger forest areas. However, multispectral systems with optimal sensor characteristics (e.g., band position and bandwidth) are yet to be developed and validated for broader application.

Further research is needed to evaluate the robustness of these relationships across other stress contexts beyond bark beetle infestation, where hydraulic responses may be less pronounced and more difficult to detect. In addition, the limited sample size in this study constrains the statistical strength of the analyses, meaning that the regression results should be interpreted as exploratory rather than definitive. Nevertheless, the consistent patterns observed between spectral indices and sap flow dynamics provide meaningful insights and a valuable basis for future studies aimed at linking remote sensing signals with tree hydraulic functioning.

## 4. Conclusion

This study highlights the potential of GSI to reveal physiological changes associated with declining tree hydraulic functioning. By linking canopy spectral responses with sap flow dynamics, this study provides evidence that remotely sensed signals can capture key processes linked to water-related stress. These findings support the development of spectral approaches for tree health monitoring using green-shoulder indices, while emphasizing the need for further research across larger datasets and a wider range of stress conditions to confirm their robustness and operational applicability.

## Acknowledgments

This research was funded by the European Union with project RESDiNET [project grant 101078970 to LH], and the Swedish Research Council for Sustainable Development Formas [project grant 2024-00404 to LH] on the salary cost, the Forest Damage Centre at the Swedish University of Agricultural Sciences on the data collection and salary costs [project grants 260FDC05, 260FDC57, 260FDC44, 260FDC12 to LH], the Kempe Foundation on the hyperspectral drone system [project grant JCSMK22-0126 to LH], the Hildur & Sven Wingquist's Foundation for Forest Science Research on the sap flow monitoring stations [project grant 2022-117-Wingquists stiftelse].

## References

Chaves, M. M., Flexas, J., & Pinheiro, C. (2009). Photosynthesis under drought and salt stress: Regulation mechanisms from whole plant to cell. *Annals of Botany*, 103(4), 551–560. https://doi.org/10.1093/aob/mcn125

Cosimo, L. H. E., Lindberg, E., Persson, H., Bohlin, J., and Huo, L. (2025). Hyperspectral drone images indicate that green shoulder indices are robust in pre-emergence detection of spruce bark beetle infestation across spatial and temporal scales, *Int. Arch. Photogramm. Remote Sens. Spatial Inf. Sci.*, XLVIII-2/W11-2025, 73–79. https://doi.org/10.5194/isprs-archives-XLVIII-2-W11-2025-73-2025

D’Odorico, P., Fawcett, D., Peters, R., Steger, D., Zhorzel, T., Hoch, G., Basler, D., Ginzler, C., Eisenring, M., Glauser, G., Zweifel, R., Gessler, A., & Kahmen, A. (2025). Deciphering tree drought responses across species: Linking leaf water potentials with remote sensing greenness and photoprotection dynamics. *Agricultural and Forest Meteorology*, 375, 110856. https://doi.org/10.1016/j.agrformet.2025.110856

Gamon, J. A., Peñuelas, J., & Field, C. B. (1992). A narrow-waveband spectral index that tracks diurnal changes in photosynthetic efficiency. Remote Sensing of Environment, 41(1), 35–44. https://doi.org/10.1016/0034-4257(92)90059-S
Grünig, M. et al. (2026). Climate change will increase forest disturbances in Europe throughout the 21st century. *Science*, 391, eadx6329.

Huo, L., Koivumäki ,Niko, Näsi ,Roope, & and Honkavaara, E. (2025). Sensitivity analysis of the Green Shoulder indices in pre-emergence detection of single trees attacked by European spruce bark beetle. *International Journal of Remote Sensing*, 46(9), 3513–3525. https://doi.org/10.1080/01431161.2025.2482747

Huo, L., Koivumäki, N., Oliveira, R. A., Hakala, T., Markelin, L., Näsi, R., Suomalainen, J., Polvivaara, A., Junttila, S., & Honkavaara, E. (2024). Bark beetle pre-emergence detection using multi-temporal hyperspectral drone images: Green shoulder indices can indicate subtle tree vitality decline. *ISPRS Journal of Photogrammetry and Remote Sensing*, 216, 200–216. https://doi.org/10.1016/j.isprsjprs.2024.07.027

Lopez, J. G., Pypker, T., Licata, J., Burgess, S. S. O., & Asbjornsen, H. (2021). Maximum heat ratio: Bi-directional method for fast and slow sap flow measurements. Plant and Soil, 469(1), 503–523. https://doi.org/10.1007/s11104-021-05066-w
Mantova, M., Herbette, S., Cochard, H., & Torres-Ruiz, J. M. (2022). Hydraulic failure and tree mortality: From correlation to causation. *Trends in Plant Science*, 27(4), 335–345. https://doi.org/10.1016/j.tplants.2021.10.003

Patacca, M., Lindner, M., Lucas-Borja, M. E., Cordonnier, T., Fidej, G., Gardiner, B., Hauf, Y., Jasinevičius, G., Labonne, S., Linkevičius, E., Mahnken, M., Milanovic, S., Nabuurs, G.-J., Nagel, T. A., Nikinmaa, L., Panyatov, M., Bercak, R., Seidl, R., Ostrogović Sever, M. Z., … Schelhaas, M.-J. (2023). Significant increase in natural disturbance impacts on European forests since 1950. *Global Change Biology*, 29(5), 1359–1376. https://doi.org/10.1111/gcb.16531

Peñuelas, J., Filella, I., & Gamon, J. A. (1995). Assessment of photosynthetic radiation‐use efficiency with spectral reflectance. *New Phytologist*, 131(3), 291‐296. https://doi.org/10.1111/j.1469-8137.1995.tb03064.x

Peñuelas, J., Gamon, J. A., Fredeen, A. L., Merino, J., & Field, C. B. (1994). Reflectance indices associated with physiological changes in nitrogen- and water-limited sunflower leaves. *Remote Sensing of Environment*, 48(2), 135–146. https://doi.org/10.1016/0034-4257(94)90136-8

Romeiro, J. M. N., Eid, T., Antón-Fernández, C., Kangas, A., & Trømborg, E. (2022). Natural disturbances risks in European

Boreal and Temperate forests and their links to climate change – A review of modelling approaches. *Forest Ecology and Management*, 509, 120071. https://doi.org/10.1016/j.foreco.2022.120071

Ruban, A. V. (2016). Nonphotochemical Chlorophyll Fluorescence Quenching: Mechanism and Effectiveness in Protecting Plants from Photodamage. *Plant Physiology*, 170(4), 1903–1916. https://doi.org/10.1104/pp.15.01935

Seidl, R., Schelhaas, M.-J., Rammer, W., & Verkerk, P. J. (2014). Increasing forest disturbances in Europe and their impact on carbon storage. *Nature Climate Change*, 4(9), 806–810. https://doi.org/10.1038/nclimate2318

Tams, L., Paton, E., & Kluge, B. (2024). Urban tree drought stress: Sap flow measurements, model validation, and water management simulations. *Science of The Total Environment*, 957, 177221. https://doi.org/10.1016/j.scitotenv.2024.177221